

## THE OBSERVATIONAL DISTRIBUTION OF INTERNAL VELOCITY DISPERSIONS IN NEARBY GALAXY CLUSTERS

D. FADDA<sup>1</sup>, M. GIRARDI<sup>1</sup>  
G. GIURICIN<sup>1</sup>, F. MARDIROSSIAN<sup>1,2</sup>, AND M. MEZZETTI<sup>1</sup>

<sup>1</sup>Dipartimento di Astronomia, Università degli Studi di Trieste,  
SISSA, via Beirut 4, 34013 - Trieste, Italy,

<sup>2</sup>Osservatorio di Trieste, via Tiepolo 11, 34100 - Trieste, Italy;  
Email: fadda, girardi, giuricin, mardirossian, mezzetti @sissa.it

### ABSTRACT

We analyze the internal velocity dispersion,  $\sigma$ , of a sample of 172 nearby galaxy clusters ( $z \leq 0.15$ ), each of which has at least 30 available galaxy redshifts, and spans a large richness range. Cluster membership selection is based on nonparametric methods. In the estimate of galaxy velocity dispersion we consider the effects of possible velocity anisotropies in galaxy orbits, the infall of late-type galaxies, and velocity gradients. The dynamical uncertainties due to the presence of substructures are also taken into account.

Previous  $\sigma$ -distributions, based on smaller cluster samples, are complete for the Abell richness class  $R \geq 1$ . In order to improve  $\sigma$  completeness, we enlarge our sample by including also poorer clusters. By resampling 153 Abell-ACO clusters, according to the richness class frequencies of the Edinburgh-Durham Cluster Catalog, we obtain a cluster sample which can be taken as representative of the nearby Universe.

Our cumulative  $\sigma$ -distribution agrees with previous distributions within their  $\sigma$  completeness limit ( $\sigma \gtrsim 800 \text{ km s}^{-1}$ ). We estimate that our distribution is complete for at least  $\sigma \geq 650 \text{ km s}^{-1}$ . In this completeness range, a fit of the form  $dN \propto \sigma^\alpha d\sigma$  gives  $\alpha = -(7.4_{-0.8}^{+0.7})$ , in fair agreement with results coming from the X-ray temperature distributions of nearby clusters.

We briefly discuss our results with respect to  $\sigma$ -distributions for galaxy groups and to theories of large scale structure formation.

*Subject headings:* galaxies: clusters of – galaxies: distances and redshifts – cosmology: observations

### 1. Introduction

Galaxy clusters, which are the most massive bound galaxy systems and which have collapsed very recently or are just collapsing, play an important role in the study of large scale structure formation. In particular, the distribution of internal velocity dispersion in galaxy clusters can be a strong constraint of cosmological models (e.g. Frenk et al. 1990; Bartlett & Silk 1993; Jing & Fang 1994; Crone & Geller 1995).

The velocity dispersion (hereafter  $\sigma$ ) of a galaxy population, which is in dynamical equilibrium within the cluster and traces the whole system, is directly linked to the total gravitational potential via the virial theorem. The precise relation between mass and dispersion depends on an assumption about the relative distribution of mass and galaxies (Merritt 1987).

The observational determination of the  $\sigma$  distribution encounters several problems. Some of these arise in the estimate of  $\sigma$  and are due to, e.g., cluster member selection, velocity anisotropy in galaxy orbits, cluster asphericity, possible infall of spiral galaxies into the cluster, and the presence of substructures (see e.g. Girardi et al. 1996, hereafter G96, for a detailed discussion of these topics).

In particular, cluster velocity anisotropies are poorly known (e.g. Merritt 1987; Dejonghe 1987). In order to avoid effects of possible anisotropies on  $\sigma$  estimates, G96 suggested studying the "integral" velocity dispersion profile (hereafter VDP), where the dispersion at a given radius is evaluated by using all the galaxies within that radius.

Although the presence of velocity anisotropies can strongly influence the value of  $\sigma$  computed for the central cluster region, it does not affect the value of the spatial (or projected)  $\sigma$  computed for the whole cluster (The & White 1986; Merritt 1988). Observationally, the VDPs of several clusters show strongly increasing or decreasing behaviours in the central cluster regions, but they are flattening out in the external regions (beyond  $\sim 1 h^{-1} \text{ Mpc}$ ) suggesting that in such regions they are no longer affected by velocity anisotropies (Figure 1 of G96). Thus, while the  $\sigma$ -values computed for the central cluster region could be a very poor estimate of the depth of cluster potential wells, we can reasonably adopt the  $\sigma$  value computed by taking all the galaxies within the radius at which the VDP becomes roughly constant.

As a general result of their analysis, G96 found evidence of a fair equipartition between galaxy and gas energy, which suggests that  $\sigma$ , like the X-ray temperature of the intracluster medium, can be a good estimate of cluster potential wells.

Other problems regarding the determination of  $\sigma$ -distribution arise from the need to have a cluster sample representative of the Universe, at least above a lower limit of  $\sigma$ .

The present  $\sigma$ -distributions are based on cluster samples which are complete with respect to cluster richness but not with respect to  $\sigma$  (Frenk et al. 1990; Girardi et al. 1993; Zabludoff et al. 1993a [Z93]; Collins et al. 1995; Mazure et al. 1996 [M96]).

The samples used are generally complete for the Abell

richness class  $R \geq 1$  or for  $R$  intermediate between 0 and 1 (Abell counts  $N_c \sim 40$ ; Collins et al. 1995). Since the correlation between  $N_c$  and  $\sigma$  is very broad (e.g. Girardi et al. 1993, M96), the completeness of a sample with respect to a certain value of richness does not imply completeness of  $\sigma$ . M96 estimated that their cluster sample is complete for  $\sigma \geq 800 \text{ km s}^{-1}$ . However, they did not have any  $R < 1$  cluster in their sample. So the bias introduced by the absence of poor clusters ( $R \leq 0$ ), which is common to all previous works, calls for further analysis.

Moreover, the cluster number density is not well known and the estimate of it varies from author to author (see M96 and references therein).

The aim of this work is to obtain a  $\sigma$ -distribution based on a large cluster sample which considers also poor clusters, each cluster having a reliable  $\sigma$  estimate. In order to obtain good estimates of  $\sigma$ , we have adopted the procedure of G96, introducing some improvements described in detail in § 2. Hereafter we indicate by  $\sigma$  the line-of-sight velocity dispersion.

In § 2 we describe the data-sample and our selection procedure for cluster membership; in § 3 we compute our values of velocity dispersions; clusters with substructures are analyzed in § 4; in § 5 we obtain our  $\sigma$ -distribution; in § 6 we discuss our results and draw our conclusions.

All the errors are given at the 68% confidence level (hereafter c.l.).

A Hubble constant of  $100 h^{-1} \text{ km s}^{-1} \text{ Mpc}^{-1}$  is used.

## 2. The Data Sample

We considered 172 nearby clusters ( $z \leq 0.15$ ), each cluster having at least 30 galaxies with available redshift and showing a significant peak (see § 2.1) in the redshift space. Moreover, we considered only galaxy clusters having an error on  $\sigma \lesssim 150 \text{ km s}^{-1}$  (for  $\sigma$  computed using all the galaxies within  $1 h^{-1} \text{ Mpc}$ ). Actually, the VDPs of clusters showing larger  $\sigma$  errors are too noisy for us to understand their behaviour (§ 3).

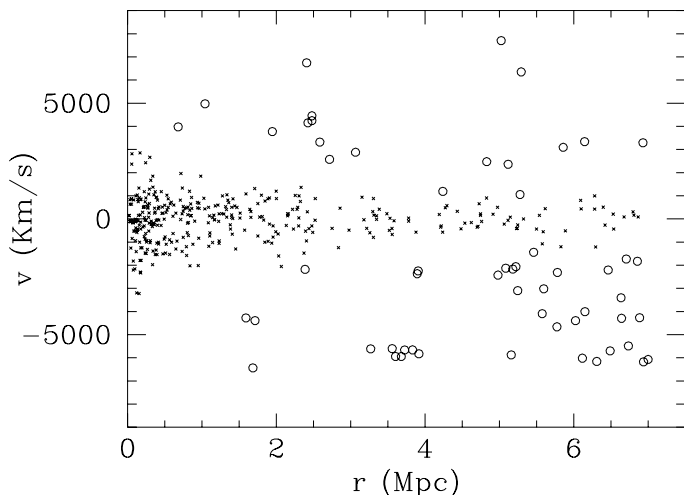


Fig. 1.—The shifting gapper method applied to the Coma cluster (A1656). The velocities are referred to the mean cluster velocity. The empty circles indicate the galaxies rejected by our procedure.

We combined data coming from the literature with new data of the ESO Nearby Abell Clusters Survey (ENACS, Katgert et al. 1996), kindly provided by the ENACS team. Most of the selected clusters (155) are Abell-ACO clusters (Abell, Corwin, & Olowin 1989). In order to achieve a sufficiently homogeneous sample, the galaxy redshifts in each cluster have usually been taken from one reference source or, if different sources were used, only when the data-sets proved to be compatible. Table 1 lists all the 172 clusters considered. In Col. (1) we list the cluster names; in Col. (2) the number of galaxies with measured redshift in each cluster field; in Col. (3) the Abell richness class for each cluster, respectively; and in Col. (4) the redshift references. The Supplementary Clusters in ACO catalog with  $N_c < 30$  are classified as belonging to  $R = -1$ .

Throughout our work we applied homogeneous procedures to the analysis of the redshifts of the clusters selected. We used robust mean and scale estimates (computed via the ROSTAT routines – see Beers, Flynn, & Gebhardt 1990), applying the relativistic correction and the usual correction for velocity errors (Danese, De Zotti & di Tullio 1980). When the correction for velocity errors leads to a negative value of  $\sigma$ , we adopted  $\sigma = 0$  with an error equal to the value of the correction. Moreover, in several analyses we used the adaptive kernel technique in one- and two-dimensions, which is a non-parametric method for detecting and analyzing galaxy systems (see Pisani 1993, 1996 and Appendix A in G96 for details). Here we may point out that, in the analysis of the velocity distribution, the method can give the significance and the position of each detected peak, as well as an estimate of overlapping between two contiguous peaks. For the sake of homogeneity, we preferred to use optical centers, which can be computed by using the two-dimensional kernel method for all clusters, at every stage of the cluster-membership selection procedure. The maps given by G96 (Figure 1) show good agreement between these optical centers and the X-ray centers. Moreover, the  $\sigma$  computed at large radii are not strongly affected by different choices of cluster center.

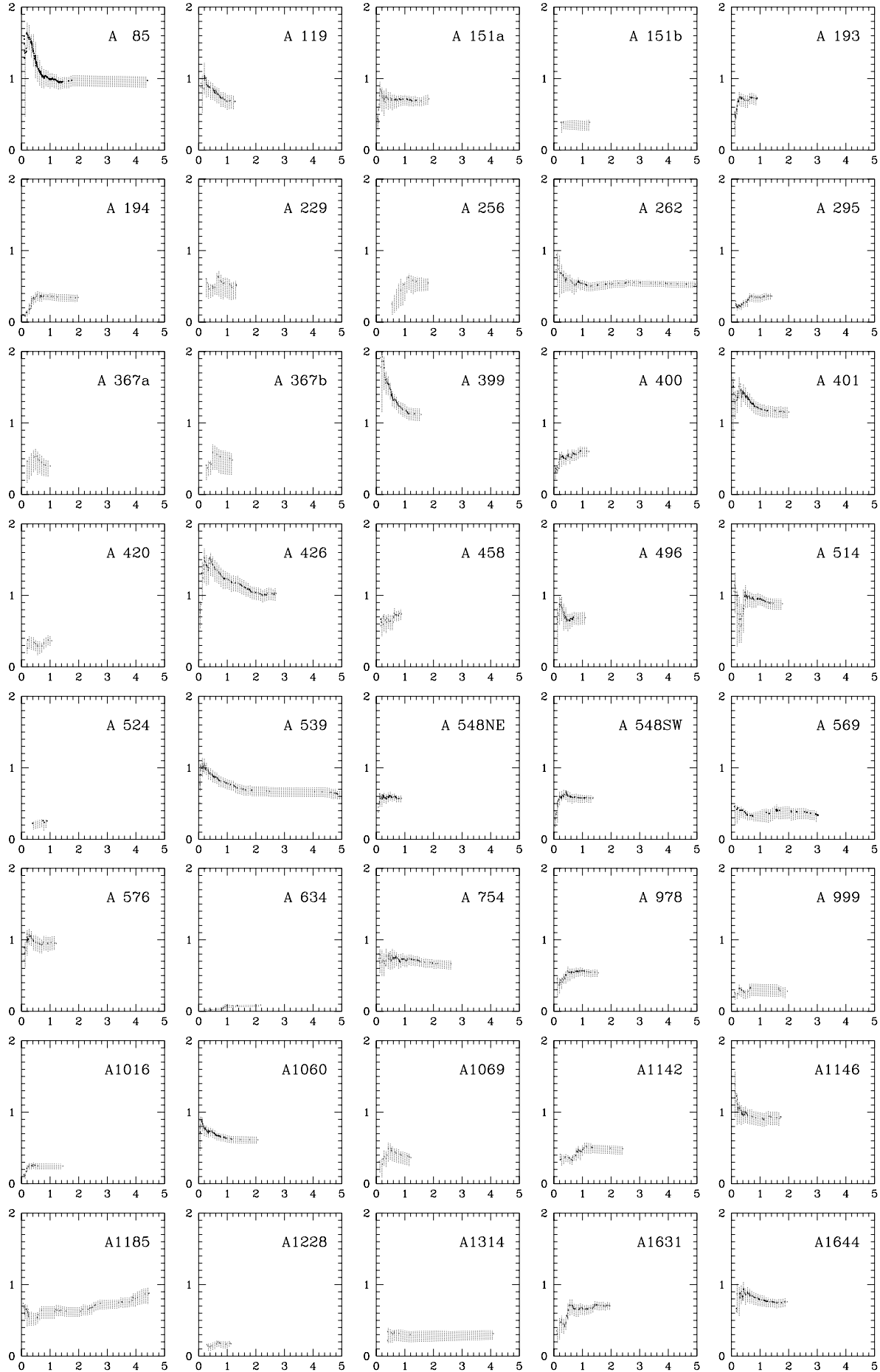
### 2.1. Selection Procedure for Cluster Membership

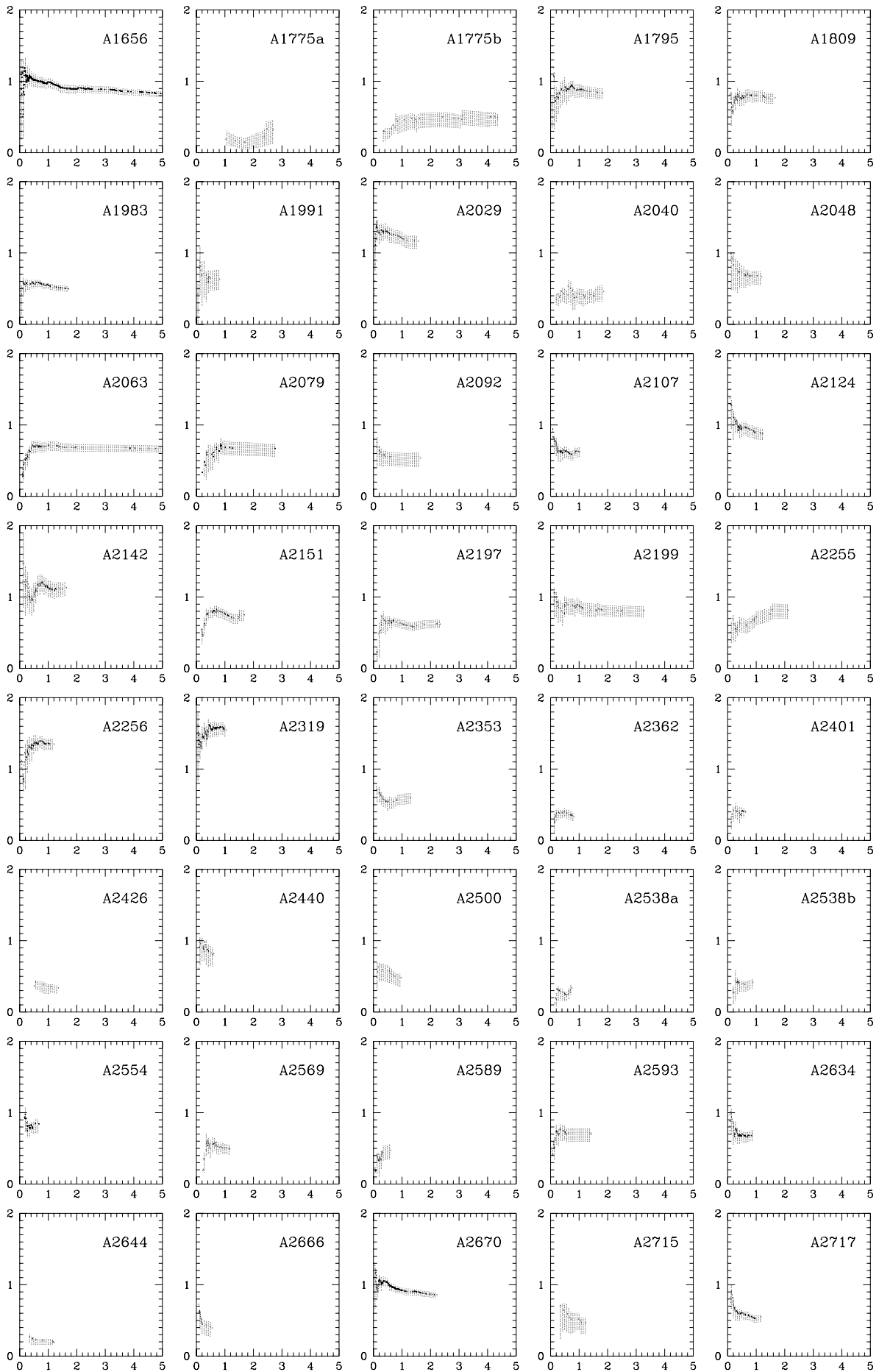
In determining cluster membership, we first used position and velocity information sequentially; then we used the two sets of data combined.

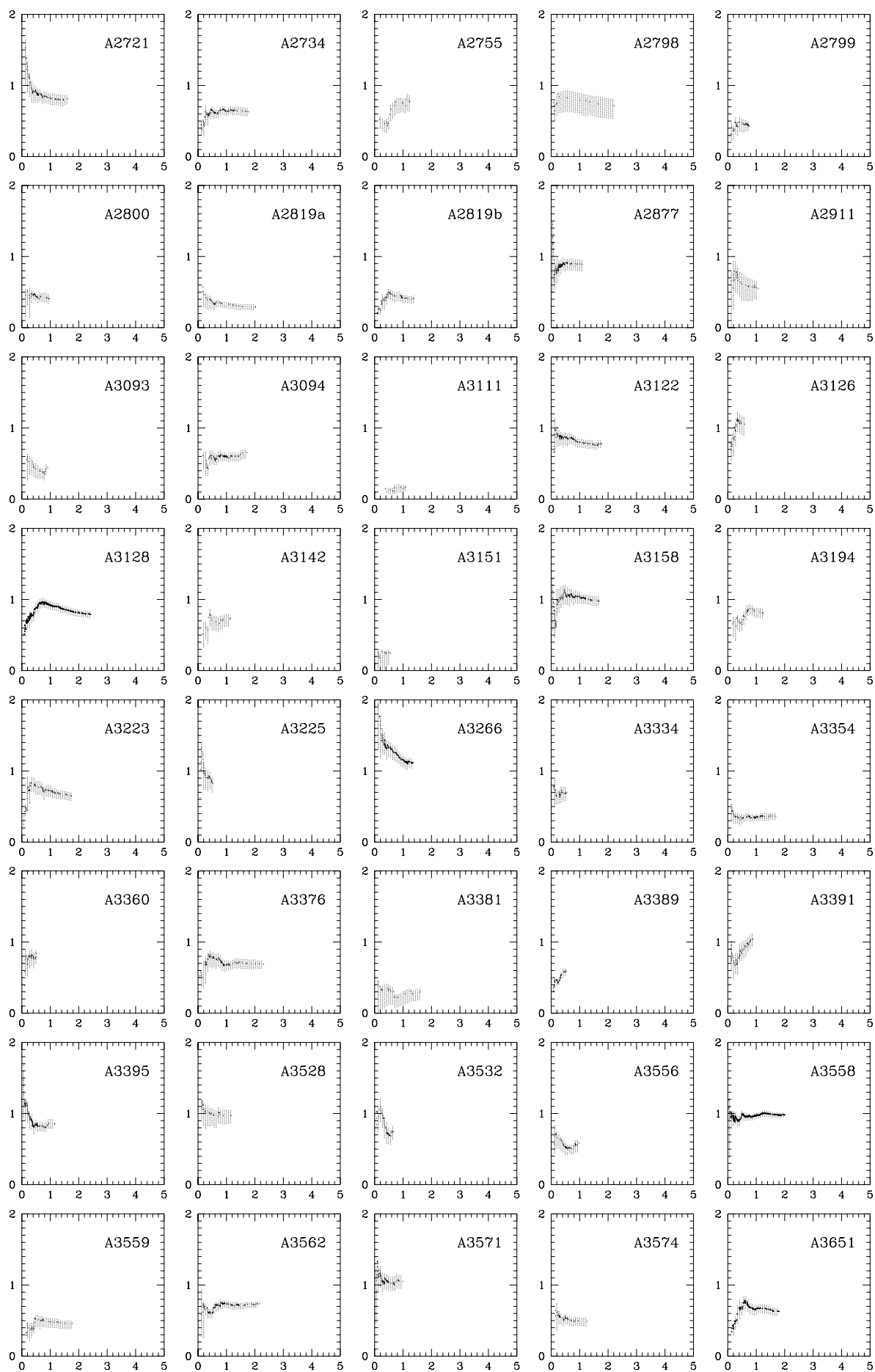
The data samples of a few clusters (A2634, A2666, A3556, A3558, and A4038) encompass large regions of the sky. So we extracted these clusters by selecting all galaxies within a fixed radius from the cluster center ( $2 h^{-1} \text{ Mpc}$  for clusters A2634 and A3558, and  $1 h^{-1} \text{ Mpc}$  for clusters A2666, A3556, A4038). In the case of clusters A399-A401 and A3391-A3395, which appear very close to one another, we selected galaxy clusters by considering their respective peaks (obtained via a two-dimensional adaptive kernel analysis). Clusters A2063 and MKW3S appear separated both in space and in redshift, according to the adaptive kernel method. We chose to separate them in redshift.

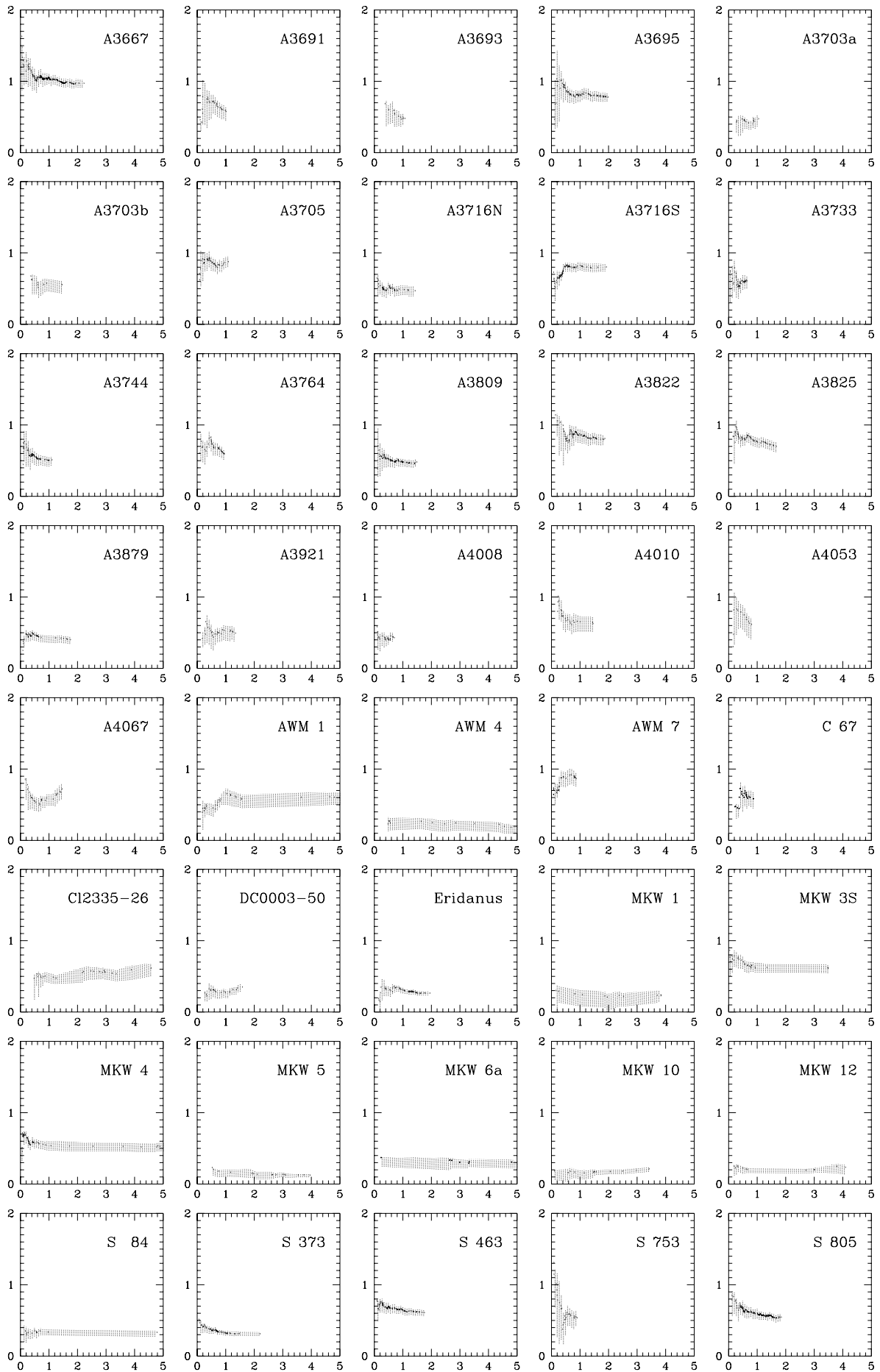
Dressler & Schectman (1988b) found that cluster A3716 is divided into two clumps (N and S clumps). Since these clumps, also evidenced by our analysis, are more distant than  $1.5 h^{-1} \text{ Mpc}$ , we decided to separate them. Cluster

A548 shows two clumps (NE and SW clumps in Dressler &









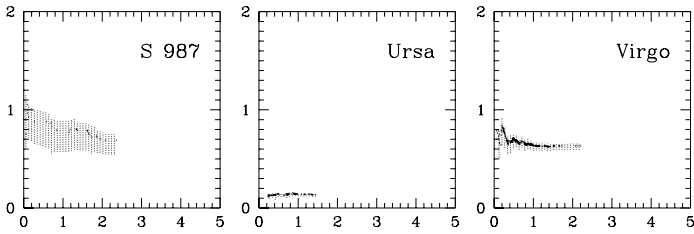


FIG. 2.—The velocity dispersion profiles (VDP), where the dispersion at a given radius is the average l.o.s. velocity dispersion within this radius. The bootstrap error bands at the 68% c.l. are shown. The distances on the x-axis are in Mpc and the velocity dispersion on the y-axis are in  $10^3 \text{ km s}^{-1}$ . (Schectman 1988b) separated by more than  $1.5 h^{-1} \text{ Mpc}$ ;

this fact is confirmed by X-ray data (Davis et al. 1995). Since the cluster also shows two peaks in the redshift distribution, we prefer to separate the two systems in redshift. The inspection of two-dimensional maps, produced via the adaptive kernel technique, does not show other obvious cases of clusters which should be subdivided.

There are several methods available in the literature for performing the usual cluster-membership selection in velocity space. For instance, the fixed gap method rejects all the galaxies separated by more than a fixed value (e.g.  $1000 \text{ km s}^{-1}$ , as used by Katgert et al. 1996) from the central body of the velocity distribution. The weighted gap method uses gaps weighted by distance from the central body (e.g. Beers et al. 1990; Girardi et al. 1993). The adaptive kernel method (Pisani 1993) is more sensitive to the presence of peaks in the velocity distribution. For instance, the cluster fields of A3526 and A539 show two peaks according to the adaptive kernel method (Pisani 1993), but the peaks in the field of A3526 are not detected by the two previous methods and the fixed gap method fails also in the case of A539.

We decided to adopt the adaptive kernel method, considering only clusters which show a significant peak (at least at the 99% c.l.). For clusters with secondary peaks, we assumed that the peaks are separable when their overlapping is  $\leq 20\%$  and their distance is  $\geq 1000 \text{ km s}^{-1}$ .

Out of 172 clusters, we found six clusters appearing as two separable peaks and 17 which are not perfectly separable according to our definition. These 17 clusters are discussed in § 4. In the following analyses we consider the remaining 155 clusters.

The combination of position and velocity information, represented by plots of velocity vs. clustercentric distance, can reveal the presence of surviving interlopers (see e.g. Kent & Gunn 1982; Regös & Geller 1989 and Figure 1). We identified them by applying the fixed gap method to a bin shifting along the distance from the cluster center. We used a gap of  $1000 \text{ km s}^{-1}$  and a bin of  $0.4 h^{-1} \text{ Mpc}$ , or a larger bin in order to have at least 15 galaxies. When the whole cluster was analyzed, we removed the interlopers. We iterated the procedure until the number of cluster members was stable. Hereafter we refer to this procedure as "shifting gapper". Our procedure has the advantage of being independent of hypotheses about the poorly known dynamical status of the cluster, while the procedure used by M96 is based on physical assumptions about the cluster mass profile.

Table 2 lists the 155 clusters which do not show any ambiguous situation of peak overlapping. In Col. (1) we list the cluster names; in Col. (2) the number of galaxies in each peak found by the adaptive kernel method; in Col. (3) the final number of galaxies used to compute the mean (galactocentric) redshift [Col. (4)], and the  $\sigma$  with bootstrap errors at the 68% c.l. [Col. (5)], for each peak.

In the above selection of cluster membership, in order to maximize the information available, we have used all the galaxies in our sample. Since the value of  $\sigma$ , used in the following analyses, depends both on galaxy velocities and on the spatial distribution, it would be better to have samples complete up to a limiting magnitude. Therefore, we have rejected the faintest galaxies of a few clusters so as to eliminate an apparent trend of the limiting magnitude to vary with the clustercentric distance.

Moreover, we did not consider galaxies beyond  $5 h^{-1} \text{ Mpc}$  from the cluster center.

## 2.2. The Effect of Late-Type Galaxies

For several clusters considered, there is only partial information regarding galaxy morphology. For 40 clusters we have both a sufficient number of early-type galaxies (ellipticals and lenticulars) and of late-type galaxies (spirals and irregulars). We checked for different means and variances in the velocity distribution of these galaxy populations by applying the standard means- and F-test (Press et al. 1992, see also G96). In order to consider the possible variation of  $\sigma$  with distance from the cluster center, in the above tests we considered only the largest area occupied by both galaxy populations. We found that 12 of the 40 clusters show evidence of kinematical differences (at the 95% c.l.).

For several other clusters, in particular ENACS clusters, we have at least some information regarding spectral features, e.g. the presence of emission lines, A-type spectra, and starburst spectra, which can be taken as indications of a late morphological type. In particular, the analysis of ENACS data shows that emission-line galaxies are generally spirals and that their  $\sigma$  within a cluster is larger than the  $\sigma$  of the other galaxies of the cluster (Biviano et al. 1996). Therefore, we repeated the above analysis, considering also spectral information for galaxies whose morphological type was unknown. All emission-line (A-type spectra, starburst spectra) galaxies were treated as late-type galaxies and all galaxies without these spectral features were grouped together with early-type galaxies. We found other eight clusters showing a kinematical difference between the two galaxy populations.

Table 3 lists the 20 clusters out of the 79 analyzed that show significant kinematical differences. In Col. (1) we list the cluster names; in Cols. (2) and (3) the number of early- and late-type galaxies used for each cluster; in Cols. (4) and (5)  $P_m$  and  $P_F$ , the probabilities that mean values and velocity dispersions of early- and late-type galaxy velocity distributions may be different, according to the mean- and F-tests, respectively; in Col. (6) the relevant morphology reference sources.

The kinematical difference between early- and late-type galaxy populations may be induced either by the presence of infall of spirals on the cluster, or by spiral-rich substructures, or by some remaining interlopers. By supposing

that cluster dynamics is better represented by early-type galaxies, we considered only this galaxy population when we found significant kinematical differences (at the 95% c.l.).

Here we are interested in determining the effect of neglecting morphological/spectral information. Of the 79 clusters analyzed, only 14 show a difference in  $\sigma$ . For these clusters, the  $\sigma$  value computed by using the global population is larger by  $87 \pm 18 \text{ km s}^{-1}$ , on average, with respect to the  $\sigma$  value computed by using only early-type galaxies. This difference is lower than that estimated by G96 in their sample, maybe because of the better interloper rejection, and it is roughly comparable within error estimates (see Table 2). For another 58 clusters, we have at least a sufficient number of early-type galaxies to compute  $\sigma$ , which is, on average,  $14 \text{ km s}^{-1}$  lower than  $\sigma$  computed for the global population. Thus our analysis, which deals with about 80% of the cluster sample, shows that the morphological effect, although possibly relevant for a few clusters, is negligible for  $\sigma$ -distribution.

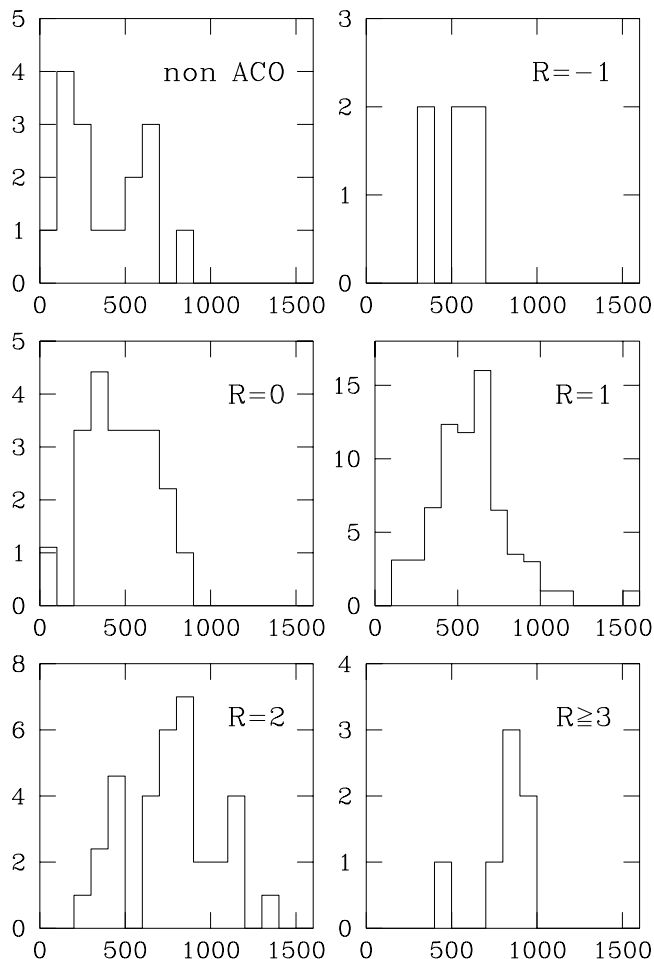


Fig. 3.—The  $\sigma$ -distributions for non Abell-ACO clusters and for clusters belonging to different Abell richness classes  $R$ . The velocity dispersions on the x-axis are in  $\text{km s}^{-1}$ .

### 3. VDP and $\sigma$ Estimates

We checked the presence of velocity gradients in the cluster velocity field, performing a multiple linear regression between the galaxy velocities and positions, and we evaluated their significance as in G96. These velocity gradients may be produced by asymmetrical effects, e.g. the presence of internal substructures, possible cluster rotation, the presence of other structures on larger scales such as nearby clusters, surrounding superclusters, filaments. For the 27 clusters having significant gradients, we applied a correction by subtracting the velocity gradient from each galaxy velocity and renormalizing the velocities so as to leave their average velocity unchanged. This correction results in an average decrease in  $\sigma$  of  $74 \pm 10 \text{ km s}^{-1}$ .

Finally, we considered the VDP, which, at a given radius is the average l.o.s. velocity dispersion within this radius, i.e. it is evaluated by using the velocities of all the galaxies within this radius (see Figure 2). The VDPs may present different behaviours in the central regions ( $\lesssim 1 h^{-1} \text{ Mpc}$ ), which may probably depend also on the choice of cluster center. However, most VDPs become flat in the external cluster regions. This suggests that the final value of VDP is representative of the total kinetic energy of galaxies. So we adopt the final value of VDP, i.e. the velocity dispersion computed by using all the cluster galaxies, as the value of  $\sigma$  except for the following cases.

Four clusters (A2440, A3225, A3691, A3764) show VDPs which appear very far from flatness in the external sampled region, but they show a sharp decrease, so we regard the final value of  $\sigma$  as being only an upper limit.

The VDPs of clusters A3391 and A4067, after the usual decreasing behaviour, show an increase in the external region. Similarly, the VDPs of clusters A1185 and AWM1 show a slowly increasing trend in the external region. This anomalous VDP increase in the external cluster region can be explained by the presence of galaxies, which survived our rejection procedure, belonging to a nearby cluster or to the field. In fact, the VDP of cluster A3391 is shown to be affected by the presence of a nearby cluster (see G96). For these four clusters we adopted the value of  $\sigma$  obtaining before the increase in VDPs towards external regions.

The VDP of the very rich cluster A2255 is particularly anomalous since it always increases, possibly becoming flat only at about  $1.5\text{-}2 h^{-1} \text{ Mpc}$ , well beyond the usual region (see e.g. the cluster A2063). The scarcity of data does not allow us to be more precise regarding this cluster, so we prefer to reject it from our list.

The  $\sigma$  values for our clusters are presented in Table 2.

M96 found no clusters with  $\sigma > 1200 \text{ km s}^{-1}$ , while in our sample we found two clusters with very high  $\sigma$  (A2256, A2319), which are not present in the M96 sample. M96 claimed that their cluster-membership selection procedure is decisive in reducing the estimate of  $\sigma$ ; in particular they compare their procedure with that used by Z93. We therefore checked our procedure against that of M96, comparing  $\sigma$  for the galaxy systems that the two samples have in common. Among these, eight clusters are recognized as being multiple peaks (in redshift or spatially) by our procedure and so our  $\sigma$  values are clearly lower than M96 values. For the other 66 systems in common, there is good agreement ( $\langle \sigma_{\text{M96}} - \sigma_{\text{our}} \rangle = 9 \pm 7 \text{ km s}^{-1}$ ) between the  $\sigma$  of M96 and ours, computed after peak selection and the "shifting gapper" procedure. Our further analyses generally reduce



the adopted value of  $\sigma$ , so that  $\langle \sigma_{M96} - \sigma_{our} \rangle = 41 \pm 10$  km s<sup>-1</sup>. This comparison suggests that our high  $\sigma$  values are not induced by our procedure. However, the value of  $\sigma = 1545$  km s<sup>-1</sup> for cluster A2319 is anomalous for its Abell class,  $R = 1$ , lying beyond 4 standard deviations from the mean (see Table 6). So we exclude it in the computation of the  $\sigma$ -distribution, although it would not cause any significant variation in the high- $\sigma$  tail of the distribution.

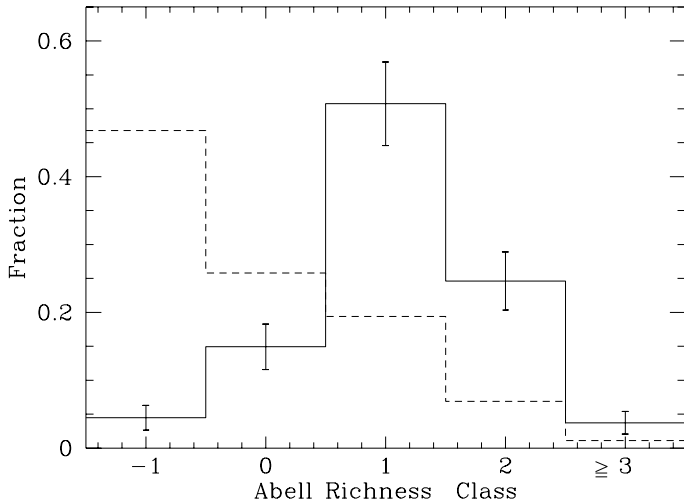


Fig. 4.—The Abell richness class distribution for our sample (solid line) and for the EDCC catalog (dashed line). The  $R$ -distribution of the EDCC catalog was obtained by re-scaling the EDCC richness to the Abell-ACO ones (see also Biviano et al. 1993).

#### 4. Cluster Substructures and Multi-peaked Clusters

Although the existence of cluster substructures is well established, it is not yet well understood to what extent it influences cluster dynamics (e.g. Fitchett 1988; González-Casado, Mamon, & Salvador-Solé 1994; West 1994). Here we take into account the possible presence of cluster substructures which can strongly modify the estimate of  $\sigma$ .

The strongly overlapping peaks presented by 17 of our clusters in their velocity distribution may have several explanations. The peaks may be different systems superimposed along the line of sight. For instance, Lucey, Currie, & Dickens (1986) found that at least a minority of galaxies in the secondary peak in cluster A3526 is actually distant from the primary peak. Otherwise, the peaks we find could indicate the presence of substructures in a single system and, in this case, it is uncertain whether we should choose between the  $\sigma$  of the substructures and the  $\sigma$  of the whole system as an indicator of the total cluster potential. Thus, we prefer to treat these multi-peaked clusters in two ways: both disjoining and not disjoining the peaks, in order to obtain two boundary limits for the true  $\sigma$ -distribution.

In order to compute  $\sigma$  for the 17 clusters, we repeated all the above analyses relative to galaxy morphology and velocity gradients. Since the dynamics of these clusters is probably more troublesome than usual, we simply adopted the value of  $\sigma$  computed for the whole galaxy sample. In Tables 4 and 5 we list the 17 clusters which show an

ambiguous situation of peak overlapping, considering the peaks as joined and disjoined, respectively. In Col. (1) we list the cluster names; in Col. (2) the number of galaxies in each peak found by the adaptive kernel method; in Col. (3) the final number of galaxies used to compute the mean (galactocentric) redshift [Col. (4)], and the  $\sigma$  with bootstrap errors at the 68% c.l. [Col. (5)], for each peak.

#### 5. The $\sigma$ -Distribution

Our cluster sample, as it spans a larger range of richness than other studies, allows us to better analyze the bias introduced by the  $R$  completeness limit. We exclude from this analysis the multi-peaked clusters.

The non Abell-ACO clusters span a large range of  $\sigma$  (see Figure 3), confirming that the Abell-ACO catalog has not detected some rich clusters. This fact was widely discussed by some authors (e.g. Scaramella et al. 1991) who pointed out that the Abell-ACO catalog is incomplete. In particular, Lumsden et al. (1992) showed that the ACO incompleteness is larger for poorer clusters. For this reason, we prefer to use the richness class distribution of the Edinburgh-Durham Cluster Catalog (EDCC, Lumsden et al. 1992), rather than that of Abell-ACO.

Table 6 lists the average value of  $\sigma$  for each  $R$ . With the present data, the  $R = -1$  class does not appear to be different from the  $R = 0$  class. The average  $\sigma$  significantly increases with  $R$  in the range  $R = 0 - 2$ , but hints at a possible flattening of this relation for  $R \geq 3$  (see also Danese et al. 1980; Girardi et al. 1993). Moreover, there is a large overlapping in  $\sigma$  values for clusters of different  $R$  (see Figure 3). For instance, in the range 800-900 km s<sup>-1</sup> we found that the ratio of the number of clusters with  $R = 0$  to the number of these with  $R \geq 1$  is about 23%, weighting such numbers by the class frequencies of the EDCC catalog. This ratio increases to 43% in the range 700-800 km s<sup>-1</sup>. This suggests a considerable incompleteness already for  $\sigma < 800 - 900$  km s<sup>-1</sup>, when the cluster sample is only complete down to  $R = 1$ .

In order to extend the  $\sigma$  completeness of the  $\sigma$ -distribution, one must consider also  $R \leq 0$  clusters. Our aim is to obtain a cluster sample representative of the nearby Universe and complete for poor clusters.

Unfortunately, our  $R$ -distribution is biased towards richer clusters with respect to the EDCC catalog (see Figure 4), which is claimed to be complete also for very poor clusters (Lumsden et al. 1992). We obtained a more representative cluster sample by resampling our clusters to mimic an universal  $R$ -distribution (see also Girardi et al. 1993; Biviano et al. 1993). We computed the  $\sigma$ -distribution by using 10000 random extractions of observed  $\sigma$ , distributed according to the EDCC  $R$ -distribution. In order to take into account the upper limited values, we redistributed the upper limits among the lower detected values. In the case of clusters with  $n$  peaks, the value of  $\sigma$  of each peak is weighted by  $1/n$ . The same weighting was also used to compute the  $\sigma$  averages presented in Table 6 and to obtain the histograms in Figure 3.

We applied the resampling procedure to the 148 Abell-ACO  $R \geq 0$  clusters. The ambiguity of clusters with uncertain dynamics (§ 4) results in two  $\sigma$ -distributions.

These cumulative  $\sigma$ -distributions and the one obtained by weighting the two cases in the same way are plotted in Figure 5. The upper and lower cumulative distributions are so close that they lie well within the error bands of the intermediate one. Therefore, in the following analyses we adopt the intermediate distribution as the  $\sigma$ -distribution complete for  $R \geq 0$  clusters.

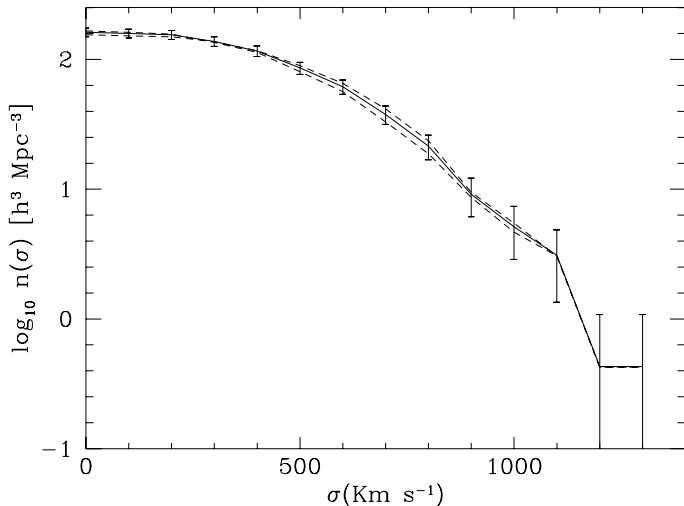


Fig. 5.—The cumulative  $\sigma$ -distributions for  $R \geq 0$  clusters. The dashed lines consider multip peaked clusters as treated in Tables 4 and 5. The intermediate case (solid line) is represented with its error bars.

In order to further extend the completeness of our  $\sigma$ -distribution, we considered all the 153 clusters with  $R \geq -1$ . Since we found no difference in mean  $\sigma$  between  $R = 0$  and  $R = -1$  clusters, and we had a small number of  $R = -1$  clusters, we treated these two classes together. We again applied the above procedure, now obtaining a  $\sigma$ -distribution complete for  $R \geq -1$  clusters.

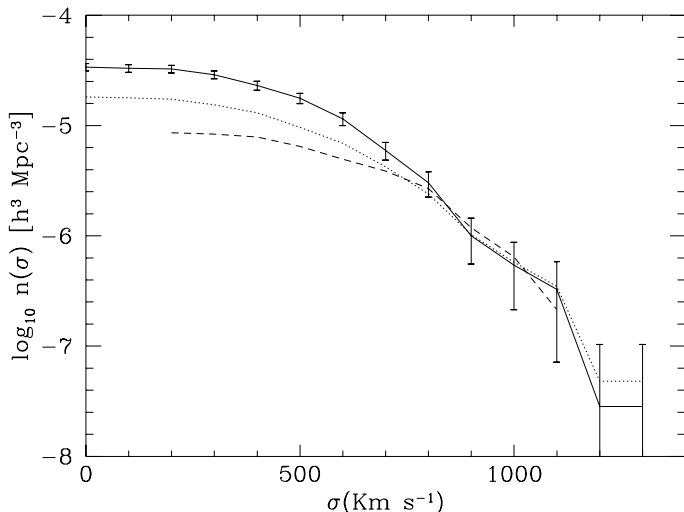


Fig. 6.—The comparison of cumulative  $\sigma$ -distributions: our results for  $R \geq -1$  clusters (solid line) and for  $R \geq 0$  clusters (dotted line); M96 for clusters with  $R \geq 1$ , (dashed line).

To normalize our distributions we adopted the cluster volume density  $8.6 \cdot 10^{-6} h^{-1} Mpc^{-3}$  for clusters with  $R \geq 1$  (M96) scaled to the EDCC class frequencies. The M96 value was corrected for the incompleteness of the Abell-ACO catalog with respect to the EDCC catalog, so that our normalization is consistent with our procedure.

Figure 6, which compares our cumulative distribution with that of M96, shows how the better  $R$ -completeness of our cluster sample improves the sample completeness with respect to  $\sigma$ . The Kolmogorov-Smirnov test assures that our  $\sigma$ -distribution, complete for  $R \geq 0$  ( $R \geq -1$ ) clusters, is not significantly different from the less  $R$ -complete ones, presented in recent works (Girardi et al. 1993; Z93; Collins et al. 1995; M96), within their supposed completeness limit ( $\sigma \sim 800 \text{ km s}^{-1}$ ). The estimate of the (better) completeness limit of our  $\sigma$  distribution requires other analyses.

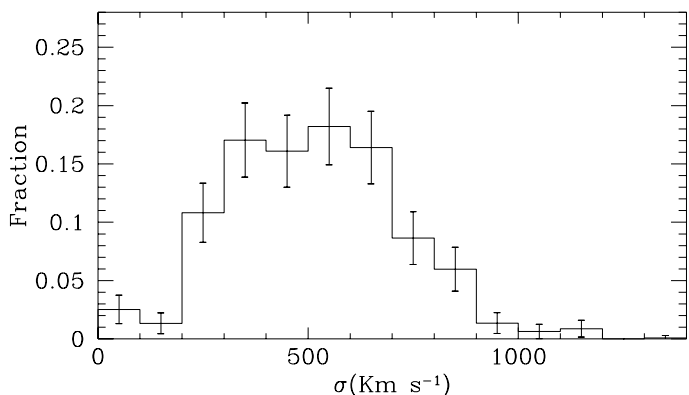


Fig. 7.—The  $\sigma$ -distribution of clusters with  $R \geq -1$ .

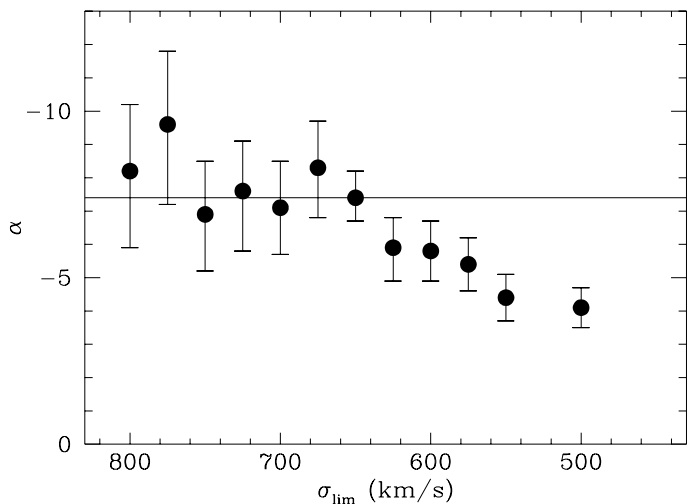


Fig. 8.—The exponents  $\alpha$  of the fitted power law obtained from fitting in larger and larger ranges ( $\sigma \geq \sigma_{lim}$ ). The horizontal line shows the  $\alpha$  value adopted in this paper.

The inspection of our  $\sigma$ -distribution (Figure 7) shows an obvious incompleteness below  $\sigma \sim 500 \text{ km s}^{-1}$ . We fitted our data to a power law ( $dN \propto \sigma^\alpha d\sigma$ ) by using the Maximum Likelihood method. We made this fit in differ-

ent ranges by decreasing the supposed completeness limit from  $800 \text{ km s}^{-1}$  to  $500 \text{ km s}^{-1}$ . The exponent  $\alpha$  appears to be roughly stable, within the errors, down to a limiting value of about  $650 \text{ km s}^{-1}$  (Figure 8). Consequently, if we assume that the  $\sigma$ -distribution is well described by a power law, this value of  $\sigma$  represents our completeness limit. The fit in this range, acceptable according to the Kolmogorov-Smirnov test, gives  $\alpha = -(7.4_{-0.8}^{+0.7})$ .

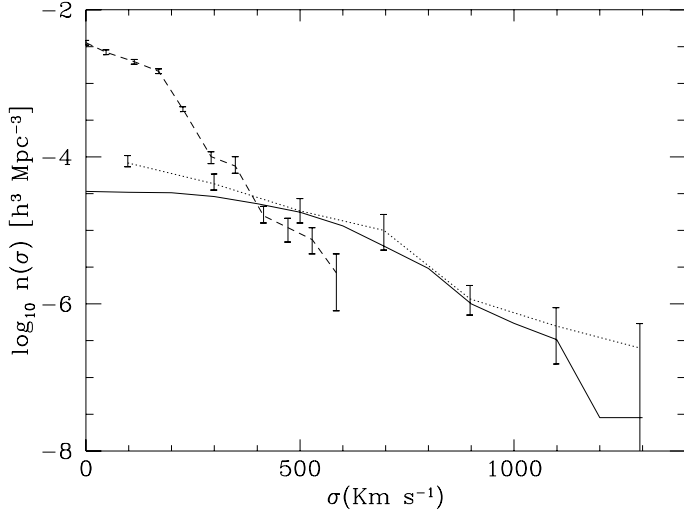


Fig. 9.—The comparison of cumulative  $\sigma$ -distributions: our results for  $R \geq -1$  clusters (solid line); Zabludoff et al. (1993a) for groups and clusters (dotted line); Moore et al. (1993) for groups (dashed line).

## 6. Discussion and Conclusions

The  $\sigma$ -values we present here were obtained by taking into account the effects which could modify the final  $\sigma$ -distribution. In particular, our  $\sigma$  values are independent of possible velocity anisotropy in galaxy orbits. The distribution of spatial  $\sigma$  is recovered by applying the usual projection factor ( $\sqrt{3}$ ) which relates the line-of-sight to the spatial  $\sigma$ . Also in the presence of cluster asphericity, the projection factor, averaged over a sample of randomly oriented clusters, is still the same (see G96), so that possible errors cancel each other out in the  $\sigma$ -distribution.

At present, an extended volume-complete sample of clusters (with known  $\sigma$ ) which includes poor clusters is not available. On the other hand, one needs to take into account also poor clusters in order to obtain a better  $\sigma$  completeness. By resampling 153 Abell-ACO clusters, according to the richness class frequencies of the EDCC catalog, we obtain a cluster sample representative of the nearby Universe down to and including poor clusters.

Our  $\sigma$ -distribution agrees with previous optical results and extends the  $\sigma$  completeness limit down to at least  $650 \text{ km s}^{-1}$ . In this range, a fit of the form  $dN \propto \sigma^\alpha d\sigma$  gives  $\alpha = -(7.4_{-0.8}^{+0.7})$ .

This result agrees with the distribution functions of X-ray temperatures. By converting the X-ray temperature  $T$  to the equivalent  $\sigma$  according to the relation  $T \propto \sigma^2$ , one obtains the values of  $\alpha = -(8.86 \pm 0.74)$  and  $\alpha = -(8.4 \pm 1.0)$ , by using the results of Edge et al. (1990) and Henry & Arnaud (1991), respectively. If

one assumes the empirical relation  $T \propto \sigma^{1.64}$  obtained by G96, the agreement is even better:  $\alpha = -(7.45 \pm 0.61)$  and  $\alpha = -(7.0 \pm 0.8)$ , respectively.

In order to more fully verify the completeness of our distribution in the low  $\sigma$  range, we also considered the results for galaxy groups, as the boundary between groups and poor clusters is very fuzzy. We compared our cumulative distribution with the one obtained by Z93, who considered groups and clusters, and with that of Moore et al. (1993) who considered groups, reporting their exact cluster volume-densities (Figure 9). Considering the error bands, we agree with the Z93 distribution down to  $400 \text{ km s}^{-1}$ , well beyond our supposed completeness limit. The comparison with the  $\sigma$ -distribution of Moore et al. (1993) suggests that their volume-density of groups for  $\sigma \geq 400 \text{ km s}^{-1}$  may be underestimated with respect to the volume-density of our poor systems. Unfortunately, we cannot draw any firm conclusions about our possible incompleteness level, and hence about the behaviour of the  $\sigma$ -distribution, for  $\sigma < 650 \text{ km s}^{-1}$ , because the  $\sigma$ -distribution of galaxy groups is still poorly known. In particular, taking the groups identified by Garcia (1993) and analyzed by Giaioti et al. (1996), we verified that the shape of the  $\sigma$ -distributions strongly depends on the choice of the selection method (hierarchical, friends of friends, and a combination of the two methods, see Garcia 1993).

For the range of  $\sigma$ -distribution pertaining to clusters, there is good agreement among the results obtained by different authors. In particular, the improved statistics used in this work allow us to further reduce observational errors. Therefore, our distribution is already sufficiently extended and precise to be a good constraint for theories of large-scale structures formation. The comparison with theoretical distributions (e.g. Jing & Fang 1994; Crone & Geller 1995) allows us to reject some models, e.g. the standard cold dark matter model. However, the new COBE normalization (Górski et al. 1995) might further reduce the range of acceptable models. We have not made any comparison with theoretical mass functions, since the mass- $\sigma$  relation is still poorly known. For instance, in our case, the virial theorem relates mass and dispersion only after an assumption regarding the relative distribution of mass and galaxies.

Since observational  $\sigma$ -distributions, in spite of their uncertainties, are more reliable than mass-distributions, we stress the need for a large computational effort in order to obtain good  $\sigma$ -distributions from N-body simulations for a variety of cosmological models.

We are particularly indebted to the ENACS team for having kindly provided us with their data, based on observations collected at the European Southern Observatory (ESO), in advance of publication.

We thank Dario Giaioti, who provided us with his results on galaxy groups, Andrea Biviano, Stefano Borgani, Yi-Peng Jing, Nicola Menci, Manolis Plionis, Massimo Ramella, and Riccardo Valdarnini for useful discussions.

We thank the referee David Merritt for his useful suggestions. Some misprints in the tabulated redshifts were noted by the first anonymous referee.

This work was partially supported by the *Ministero per l'Università e per la Ricerca scientifica e tecnologica*, by

the *Italian Space Agency (A.S.I.)*, and by the *Consiglio*

*Nazionale delle Ricerche (CNR-GNA)*.

## REFERENCES

- Abell, G.O., Corwin, H. G. Jr., & Olowin, R. P. 1989, *ApJS*, 70, 1
- Bardelli, S., Zucca, E., Vettolani, G., Zamorani, G., Scaramella, R., Collins, C. A., & MacGillivray, H. T. 1194, *MNRAS*, 267, 665
- Bartlett, J. G., Silk, J. 1993, *ApJ*, 407, L45
- Beers, T. C., Flynn, K., & Gebhardt, K. 1990, *AJ*, 100, 32
- Beers, T. C., Forman, W., Huchra, J. P., Jones, C., & Gebhardt, K. 1991, *AJ*, 102, 1581
- Beers, T. C., Gebhardt, K., Huchra, J.P., Forman, W., Jones, C. & Bothun, G. D. 1992, *ApJ*, 400, 410
- Beers, T. C., Geller, M. J., Huchra, J. P., Latham, D. W., & Davis, R.J. 1984, *ApJ*, 283, 33
- Binggeli, B., Sandage, A., & Tammann, G. A. 1985, *AJ*, 90, 1681
- Biviano, A., Katgert, P., Mazure, A., Moles, M., den Hartog, R., & Focardi, P. 1996, *Astrophysical Letters and Communications*, in press (preprint astro-ph 9511050)
- Biviano, A., Girardi, M., Giuricin, G., Mardirossian, F., & Mezzetti, M. 1993, *ApJ*, 411, L13
- Bothun, D., Aaronson, M., Schommer, B., Mould, J., Huchra, J., & Sullivan, W. T. III 1985, *ApJS*, 57, 423
- Bothun, G. D., & Schombert, J. M. 1988, *ApJ*, 335, 617
- Butcher, H. R., & Oemler, A. Jr. 1985, *ApJS*, 57, 665
- Chapman, G. N. F., Geller, M.J., & Huchra, J. P. 1987, *AJ*, 94, 571
- Chapman, G. N. F., Geller, M.J., & Huchra, J. P. 1988, *AJ*, 95, 999
- Chincarini, G., & Rood, H. J. 1976, *PASP*, 88, 388
- Chincarini, G., & Rood, H. J. 1977, *ApJ*, 214, 351
- Chincarini, G., Tarengi, M., & Bettis, C. 1981, *A&A*, 96, 106
- Colless, M., & Hewett, P. 1987, *MNRAS*, 224, 453
- Collins, C. A., Guzzo, L., Nichol, R. C., & Lumsden, S. L. 1995, *MNRAS*, 274, 1071
- Cristiani, S., de Souza, R., D'Odorico, S., Lund, G., & Quintana, H. 1987, *A&A*, 179, 108
- Crone, M. M., & Geller, M. J. 1995, *AJ*, 110, 21
- Danese, C., De Zotti, G., & di Tullio, G. 1980, *A&A*, 82, 322
- Davis, D. S., Bird, C. M., Mushotzky, R. F., & Odewahn, S. C. 1995, *ApJ*, 440, 48
- Dejonghe, H. 1987, *MNRAS*, 224, 13
- Dell'Antonio, I. P., Geller, M. J., & Fabricant, D. G. 1994, *AJ*, 107, 427
- Dickens, R. J., Currie, M. J., & Lucey, J. R. 1986, *MNRAS*, 220, 679
- Dickens, R. J., & Moss, C. 1976, *MNRAS*, 174, 47
- Dressler, A. 1980, *ApJS*, 42, 565
- Dressler, A., & Shectman, S.A. 1988a, *AJ*, 95, 284
- Dressler, A., & Shectman, S. A. 1988b, *AJ*, 95, 985
- Edge, A. C., Stewart, G. C., Fabian, A. C., & Arnaud, K. A. 1990, *MNRAS*, 245, 559
- Ettori, S., Guzzo, L., Tarengi, M. 1995, *MNRAS*, 276, 689
- Faber, S. M., & Dressler, A. 1977, *AJ*, 82, 187
- Fabricant, D. G., Kent, S. M., & Kurtz, M. J. 1989, *ApJ*, 336, 77
- Fabricant, D., Kurtz, M., Geller, M., Zabludoff, A., Mack, P., & Wegner, G. 1993, *AJ*, 105, 788
- Fitchett, M. J. 1988, in *The Minnesota Lectures on Clusters of Galaxies and Large-Scale Structure*, J.M. Dickey Ed., Bringham Young University Press, Provo.
- Frenk, C. S., White, S. D. M., Efstathiou, G., & Davis, M. 1990, *ApJ*, 351, 10
- Garcia, A. M. 1993, *A&AS*, 100, 47
- Gavazzi, G. 1987, *ApJ*, 320, 96
- Geller, M. J., Beers, T. C., Bothun, G. D., & Huchra, J. P. 1984, *AJ*, 89, 319
- Giaiotti, D., Giuricin, G., Mardirossian, F., Mezzetti, M., & Pisani, A. 1996, in preparation
- Giovanelli, R., Haynes, M. P., & Chincarini, G. L. 1982, *ApJ*, 262, 442
- Girardi, M., Biviano, A., Giuricin, G., Mardirossian, F., & Mezzetti, M. 1993, *ApJ*, 404, 38
- Girardi, M., Fadda, D., Giuricin, G., Mardirossian, F., Mezzetti, & M. Biviano, A. 1996, *ApJ*, 457, 61 [G96]
- González-Casado, G., Mamon, G. A., & Salvador-Solé 1994, *ApJ*, 433, L61
- Górski, K. M., Ratra, B., Sugiyama, N., & Banday, A. J. 1995, *ApJ*, 444, L65
- Gregory, S. A., & Thompson, L. A. 1978, *ApJ*, 222, 784
- Gregory, S. A., & Thompson, L. A. 1984, *ApJ*, 286, 422
- Gregory, S. A., Thompson, L. A., & Tifft, W. G. 1981, *ApJ*, 243, 411
- Henry, J. P. & Arnaud, K. A. 1991, *ApJ*, 372, 410
- Hill, J. M., & Oegerle, W. R. 1993, *AJ*, 106, 831
- Hintzen, P. 1980, *AJ*, 85, 626
- Hintzen, P., Hill, J. M., Lindley, D., Scott, J. S., & Angel, J. R. P. 1982, *AJ*, 87, 1656
- Hintzen, P., & Scott, J.S. 1979, *A&A*, 74, 116
- Huchra, J., Geller, M., Clemens, C., Tokarz, S., & Mickel, A. 1992, *Bull. CDS*, 41, 31
- Jing, Y. P., & Fang, L. Z. 1994, *ApJ*, 432, 438
- Katgert, P., Mazure, A., Perea, J., et al. 1996, *A&A*, in press (preprint astro-ph 9511051) - [ENACS]
- Kent, S. M., & Gunn, J. E. 1982, *AJ*, 87, 945
- Kent, S. M., & Sargent, W. L. W. 1983, *AJ*, 88, 697
- Lauberts, A., Valentijn, E.A. 1989, "The Surface Photometry Catalogue of the ESO-Uppsala Galaxies", Garching bei Munchen: ESO
- Lucey, J. R., & Carter, D. 1988, *MNRAS*, 235, 1177
- Lucey, J. R., Currie, M. J., & Dickens, R. J. 1986, *MNRAS*, 221, 453
- Lucey, J. R., Dickens, R. J., Mitchell, R. J., & Dawe, J. A. 1983, *MNRAS*, 203, 545
- Lumsden, S. L., Nichol, R. C., Collins, C. A., & Guzzo, L. 1992, *MNRAS*, 258, 1
- Malumuth, E. M., Kriss, G. A., Van Dyke Dixon, W., Ferguson, H. C., & Ritchie, C. 1992, *AJ*, 104, 495
- Mazure, A., Katgert, P., den Hartog, R. et al. 1996, *A&A*, in press (preprint astro-ph 9511052) - [M96]
- Metcalf, N., Godwin, J. G., & Spenser, S. D. 1987, *MNRAS*, 225, 581
- Merritt, D. 1987, *ApJ*, 313, 121
- Merritt, D. 1988, in *The Minnesota Lectures on Clusters of Galaxies and Large-Scale Structure*, J.M. Dickey Ed., Bringham Young University Press, Provo.
- Materne, J., & Hopp, U. 1983, *A&A*, 124, L13
- Moore, B., Frenk, C. S., & White, D. M. 1993, *MNRAS*, 261, 827
- Oegerle, W. R., & Hill, J. M. 1993, *AJ*, 104, 2078
- Oegerle, W. R., Hill, J. M., & Fitchett, M. J. 1995, *AJ*, 110, 1
- Ostriker, E. C., Huchra, J. P., Geller, M. J., & Kurtz, M. J. 1988, *AJ*, 96, 1775
- Paturel, G., Fouqué, P., Bottinelli, L., & Gouguenheim, L. 1989, *Catalogue of Principal Galaxies, Observatoire de Lyon (PGC)*
- Pinkney, J., Rhee, G., & Burns, J. O. 1993, *ApJ*, 416, 36
- Pisani, A. 1993, *MNRAS*, 265, 706
- Pisani, A. 1996, *MNRAS*, 278, 697
- Postman, H., Huchra, J. P., M., & Geller, M. J. 1986, *AJ*, 92, 1238
- Press, W. H., Teukolsky, S. A., Vetterling, W. T., & Flannery, B. P. 1992, in *Numerical Recipes (Second Edition)*, (Cambridge University Press)
- Regös, E., & Geller, M. J. 1989, *AJ*, 98, 755
- Proust, D., Quintana, H., Mazure, A., da Souza, R., Escalera, E., Sodré, L. Jr., & Capelato, H. V. 1992, *A&A*, 258, 243
- Quintana, H., & de Souza, R. 1993, *A&AS*, 101, 475
- Quintana, H., Melnick, J., Infante, L., & Thomas, B. 1985, *AJ*, 90, 410
- Quintana, H., & Ramirez, A. 1990, *AJ*, 100, 1424
- Richter, O. G. 1987, *A&AS*, 67, 237
- Richter, O. G. 1987, *A&AS*, 261, 266
- Richter, O. G. 1989, *A&AS*, 77, 237
- Richter, O.G., & Huchtmeier, W. K. 1982, *A&A*, 109, 155
- Scaramella, R., Zamorani, G., Vettolani, G., & Chincarini, G. 1991, *AJ*, 101, 342
- Scodreggio, M., Solanes, J. M., Giovanelli, R., & Haynes, M. P. 1995, *ApJ*, 444, 41
- Sharples, R. M., Ellis, R. S., & Gray, P. M. 1988, *MNRAS*, 231, 479
- Sodré, L., Capelato, H. V., Steiner, J. E., Proust, D., & Mazure, A. 1992, *MNRAS*, 259, 233
- Stauffer, J., Spinrad, H., & Sargent, W. L. W. 1979, *ApJ*, 228, 379
- Stepanyan, Dzh. A. 1984, *Astrophysics*, 20, 478
- Teague, P. F., Carter, D., & Gray, P. M. 1990, *ApJS*, 72, 715
- The, L.S., & White, S. D. M. 1986, *AJ*, 92, 1248
- Tifft, W. G. 1978, *ApJ*, 222, 54
- Tully, R.B. 1988, "Nearby Galaxy Catalog" (Cambridge: CUP)
- West, M. J. 1994, in *Clusters of Galaxies*, eds. F. Durret, A. Mazure, & J. Tran Thanh Van, Editions Frontieres, 23
- Willmer C. N. A., Focardi P., Chan R., Pellegrini P. S., & Nicolaci Da Costa L. 1991, *AJ*, 101, 57
- Willmer C.N.A., Focardi P., Nicolaci Da Costa L., Pellegrini P.S. 1989, *AJ*, 98, 1531
- Zabludoff, A. I., Huchra, J. P., & Geller, M. J. 1990, *ApJS*, 74, 1
- Zabludoff, A. I., Geller, M. J., Huchra, J. P., & Ramella, M. 1993a, *AJ*, 106, 1301 [Z93]
- Zabludoff, A. I., Geller, M. J., Huchra, J. P., & Vogeley, M. S. 1993b, *AJ*, 106, 1273

TABLE 1  
THE CLUSTER SAMPLE

Name (1)	N (2)	R (3)	References (4)	Name (1)	N (2)	R (3)	References (4)
A13	44	2	E	A2142	119	2	Oeg110,1;Hin74,116
A85	185	1	Bee102,1581;Mal104,495	A2151 Hercules	105	2	Dre95,284
A87	42	1	E	A2197	45	1	Gre286,422
A118	38	1	E	A2199	71	2	Gre286,422
A119	142	1	E;Fab105,788	A2255	31	2	Sta228,379
A151	142	1	E;Pro258,243	A2256	89	2	Fab336,77
A168	111	2	E;Fab82,187;Zab106,1273	A2319	128	1	Oeg110,1
A193	65	1	Hil106,831	A2353	31	1	E
A194	267	0	Cha95,999	A2362	33	1	E
A229	39	1	E	A2401	30	1	E
A256	36	1	Zab106,1273	A2426	36	2	E
A262	88	0	Gio262,442;Gre243,411	A2440	30	0	Bee102,1581
A295	65	1	E;Huc41,31;Zab106,1273	A2500	36	1	E
A367	30	1	E	A2538	45	1	Col224,453
A399	90	1	Hil106,831	A2554	41	3	Col224,453
A400	109	1	Bee400,410	A2569	41	1	E
A401	117	2	Hil106,831	A2589	33	0	Bee102,1581
A420	33	1	E	A2593	37	0	Bee102,1581
A426 Perseus	200	2	Ken88,697	A2634	315	1	Sco444,41;Hin85,626; Pin416,36; Zab74,1; Bot335,617;But57,665
A458	45	2	Col224,453				
A496	166	1	Mal104,495;Qui100,1424	A2644	35	1	E
A514	111	1	E	A2666	27	0	Sco444,41
A524	43	1	E	A2670	303	3	Sha231,479
A539	289	1	Ost96,1775	A2715	34	2	E
A548	134	1	Dre95,284	A2717	81	1	E;Col224,453
A569	41	0	Bee102,1581	A2721	104	3	Tea72,715;Col224,453
A576	51	1	Hin87,1656	A2734	116	1	E
A634	38	0	Ste20,478	A2755	36	2	E
A754	89	2	Dre95,284	A2798	31	1	Col274,1071
A957	54	1	E;Bee102,1581	A2799	42	1	E
A978	73	1	E	A2800	46	1	E
A999	45	0	Cha94,571	A2819	124	2	E
A1016	44	0	Cha94,571	A2854	35	1	E
A1060 Hydra	177	1	Ric67,237;Ric77,237	A2877	110	0	Mal104,495
A1069	40	0	E	A2911	44	1	E
A1142	66	0	Gel89,319	A3093	40	2	E
A1146	84	4	Tea72,715	A3094	99	2	E
A1185	77	1	Bee102,1581	A3111	48	1	E
A1228	39	1	Zab106,1273	A3112	128	2	E;Mat124,L13
A1314	30	0	Del107,427;Huc41,31	A3122	119	2	E
A1367	94	2	Gav320,96;Gre222,784; Tif222,54;Dic174,47	A3126	45	1	Col224,453
A1631	90	0	Dre95,284	A3128	222	3	E;Col224,453
A1644	102	1	Dre95,284	A3142	38	1	E
A1651	62	1	Del107,427;Huc41,31	A3151	43	1	E
A1656 Coma	414	2	Ken87,945	A3158	145	2	E;Chi96,106;Luc203,545
A1736	104	0	Dre95,284	A3194	33	2	E
A1775	77	2	Oeg110,1	A3202	41	1	E
A1795	98	2	Hil106,831	A3223	110	2	E
A1809	68	1	E;Hil106,831	A3225	44	0	Col224,453
A1983	100	1	Dre95,284	A3266	172	2	Tea72,715
A1991	25	1	Bee102,1581	A3334	41	2	Col224,453
A2029	93	2	Oeg110,1	A3341	118	2	E
A2040	67	1	E;Zab106,1273	A3354	110	1	E
A2048	39	1	E	A3360	40	2	Col224,453
A2052	60	0	E;Qui90,410;Mal104,495	A3376	84	0	Dre95,284
A2063	92	1	Bee102,1581;Hil106,831	A3381	64	1	Dre95,284
A2079	32	1	Pos92,1238	A3389	45	0	Tea72,715
A2092	30	1	Pos92,1238	A3391	65	0	Tea72,715
A2107	75	1	Oeg104,2078	A3395	143	1	Tea72,715
A2124	67	1	Hil106,831	A3526 Centaurus	301	0	Dic220,679;ESO

TABLE 1—*Continued*

Name (1)	N (2)	R (3)	References (4)	Name (1)	N (2)	R (3)	References (4)
A3528	39	1	E	A4038	99	2	Ett276,689;Luc235,1177
A3532	44	0	Cri179,108	A4053	31	1	E
A3556	54	0	Bar267,665	A4067	41	1	Tea72,715
A3558 Shapley 8	398	4	E;Bar267,665;Ric261,266; Tea72,715;Met225,581	S84	30	-1	Col274,1071
A3559	69	3	E	S373	57	-1	ESO
A3562	119	2	E	S463	100	-1	Dre95,284
A3571	72	2	Qui101,475	S753	43	-1	Wil101,57
A3574	42	0	Wil101,57	S805	154	-1	Mal104,495
A3651	92	1	E	S987	40	-1	Col274,1071
A3667	177	2	E;Sod259,233	AWM1	56	—	Bee283,33
A3691	36	2	E	AWM4	59	—	Del107,427;Huc41,31
A3693	33	1	E	AWM7	33	—	Del107,427;Huc41,31
A3695	96	2	E	C67	45	—	Col224,453
A3703	32	1	E	CL2335-26	38	—	Sco444,41
A3705	45	2	Col224,453	DC0003-50	55	—	Dre95,284
A3716	138	1	Dre95,284;Col224,453	Eridanus	65	—	Wil98,1531
A3733	44	1	E	MKW1	39	—	Bee283,33
A3744	86	1	E	MKW3S	30	1	Bee102,1581;Hil106,831
A3764	43	1	E	MKW4S	39	—	Del107,427;Huc41,31
A3806	119	2	E	MKW5	44	—	Del107,427;Huc41,31
A3809	127	1	E	MKW6A	37	—	Del107,427;Huc41,31
A3822	101	2	E	MKW10	69	—	Del107,427;Huc41,31
A3825	90	1	E	MKW12	66	—	Bee283,33
A3879	82	2	E	Pegasus	78	—	Ric109,155;Bot57,423; Chi88,388
A3921	38	2	E	Ursa	57	—	NGC
A4008	43	1	E	Virgo	572	—	Bin90,1681
A4010	36	1	E				

NOTE.—The bibliographical references in Column 4 use a code consisting of the first three letters of the last name of the first author, followed by the journal volume number, and then, after a comma, the initial page number of the paper. For example, the paper by Girardi & al. 1993 in this code would be “Gir404,38”. The only exceptions are: E, Enacs data; ESO, the catalog of Laubert & al. 1989; NGC, the catalog of Tully 1988.

TABLE 2  
THE VALUES OF  $\sigma$

Name (1)	$N_p$ (2)	$N_{mem}$ (3)	$z$ (4)	$\sigma$ (km/s) (5)	Name (1)	$N_p$ (2)	$N_{mem}$ (3)	$z$ (4)	$\sigma$ (km/s) (5)
A85	130	125	0.0559	969 + 95/- 61	A2319	127	118	0.0553	1545 + 95/- 77
A119	128	62	0.0438	679 +106/- 80	A2353	24	24	0.1213	597 + 88/- 66
A151a	64	64	0.0537	714 + 73/- 61	A2362	24	24	0.0616	331 + 68/- 52
A151b	29	7	0.0409	385 +118/- 31	A2401	23	23	0.0581	395 + 72/- 52
A193	56	56	0.0490	723 + 78/- 61	A2426	10	10	0.0886	332 + 80/- 28
A194	143	39	0.0184	341 + 57/- 37	A2440	24	24	0.0913	819 upp. lim.
A229	34	23	0.1137	506 +165/- 64	A2500	13	13	0.0904	477 +131/- 54
A256	15	11	0.0885	545 +107/- 60	A2538a	23	23	0.0858	326 + 72/- 59
A262	86	82	0.0169	525 + 47/- 33	A2538b	18	18	0.0808	410 + 80/- 48
A295	47	47	0.0427	359 + 52/- 32	A2554	28	27	0.1118	840 +131/- 68
A367a	13	13	0.0882	394 +150/- 77	A2569	35	35	0.0816	491 + 86/- 49
A367b	13	13	0.0936	479 +207/- 79	A2589	28	28	0.0423	470 +120/- 84
A399	87	79	0.0718	1116 + 89/- 83	A2593	37	37	0.0424	698 +116/- 69
A400	98	58	0.0237	599 + 80/- 65	A2634	217	69	0.0316	700 + 97/- 61
A401	107	106	0.0737	1152 + 86/- 70	A2644	12	12	0.0693	179 + 48/- 21
A420	15	15	0.0860	360 + 70/- 66	A2666	21	21	0.0280	383 +150/- 75
A426	200	113	0.0178	1026 +106/- 64	A2670	235	197	0.0767	852 + 48/- 35
A458	32	30	0.1057	736 + 86/- 58	A2715	13	13	0.1145	463 +152/- 72
A496	149	55	0.0325	687 + 89/- 76	A2717	57	55	0.0498	541 + 65/- 41
A514	95	81	0.0714	882 + 84/- 64	A2721	75	74	0.1152	805 + 74/- 63
A524	14	8	0.0797	250 + 62/- 32	A2734	83	80	0.0625	628 + 61/- 57
A539	180	160	0.0284	629 + 70/- 52	A2755	20	20	0.0957	768 +139/- 84
A548NE	92	62	0.0397	571 + 54/- 40	A2798	18	18	0.1130	711 +181/-101
A548SW	74	74	0.0439	583 + 60/- 37	A2799	36	36	0.0640	422 + 76/- 57
A569	39	39	0.0201	327 + 95/- 39	A2800	31	31	0.0643	404 + 68/- 74
A576	48	47	0.0384	945 + 93/- 88	A2819a	43	33	0.0876	282 + 50/- 32
A634	15	15	0.0253	0 +223/- 0	A2819b	49	49	0.0756	410 + 59/- 44
A754	82	77	0.0535	662 + 77/- 50	A2877	97	93	0.0248	887 + 94/- 68
A978	57	55	0.0539	535 + 58/- 39	A2911	30	30	0.0816	547 +159/- 93
A999	24	24	0.0317	278 +104/- 49	A3093	22	22	0.0836	440 + 80/- 56
A1016	23	23	0.0318	244 + 43/- 32	A3094	68	67	0.0677	653 + 77/- 54
A1060	144	82	0.0126	610 + 52/- 43	A3111	12	12	0.0774	159 + 54/- 28
A1069	21	21	0.0662	360 +118/- 59	A3122	91	87	0.0605	775 + 58/- 51
A1142	43	40	0.0350	486 + 81/- 41	A3126	41	38	0.0862	1053 +164/-108
A1146	64	57	0.1422	929 +101/- 83	A3128	186	179	0.0604	789 + 51/- 44
A1185	77	21	0.0300	536 +106/- 56	A3142	21	20	0.1036	737 + 98/- 63
A1228	15	15	0.0354	168 + 47/- 36	A3151	14	14	0.0662	237 +171/- 40
A1314	13	13	0.0329	277 + 83/- 45	A3158	135	123	0.0597	976 + 70/- 58
A1631	71	71	0.0464	702 + 54/- 46	A3194	31	31	0.0977	805 + 78/- 53
A1644	91	84	0.0467	759 + 61/- 56	A3223	67	66	0.0603	647 + 67/- 54
A1656	410	283	0.0233	821 + 49/- 38	A3225	40	36	0.0563	820 upp. lim.
A1775a	28	10	0.0759	293 +196/-133	A3266	132	128	0.0599	1107 + 82/- 65
A1775b	25	25	0.0650	478 +117/- 63	A3334	30	30	0.0970	696 + 91/- 79
A1795	85	81	0.0631	834 + 85/- 76	A3354	57	57	0.0585	358 + 50/- 45
A1809	60	59	0.0789	765 + 79/- 66	A3360	36	34	0.0849	835 +114/- 82
A1983	74	74	0.0452	494 + 43/- 39	A3376	77	75	0.0465	688 + 68/- 57
A1991	23	23	0.0593	631 +147/-137	A3381	29	21	0.0382	293 +110/- 54
A2029	91	73	0.0766	1164 + 98/- 78	A3389	38	38	0.0272	595 + 63/- 47
A2040	52	28	0.0454	458 +141/-102	A3391	55	18	0.0553	663 +195/-112
A2048	25	25	0.0972	664 +116/- 65	A3395	105	99	0.0506	852 + 84/- 53
A2063	92	92	0.0350	667 + 55/- 41	A3528	28	28	0.0536	972 +110/- 82
A2079	27	26	0.0662	670 +113/- 67	A3532	43	42	0.0559	738 +112/- 85
A2092	17	17	0.0673	536 +129/- 75	A3556	44	43	0.0476	580 +100/- 73
A2107	65	65	0.0415	622 + 71/- 64	A3558	353	341	0.0480	977 + 39/- 34
A2124	65	61	0.0661	878 + 90/- 72	A3559	37	37	0.0469	456 + 78/- 44
A2142	103	86	0.0907	1132 +110/- 92	A3562	118	100	0.0478	736 + 49/- 36
A2151	101	57	0.0366	751 + 91/- 69	A3571	70	69	0.0396	1045 +109/- 90
A2197	45	45	0.0308	612 + 56/- 53	A3574	39	35	0.0158	491 + 73/- 41
A2199	70	50	0.0314	801 + 92/- 61	A3651	78	68	0.0610	626 + 60/- 53
A2255	31	25	0.0824	...	A3667	167	154	0.0566	971 + 62/- 47
A2256	87	86	0.0589	1348 + 86/- 64	A3691	33	29	0.0881	575 upp. lim.

TABLE 2—*Continued*

Name (1)	$N_p$ (2)	$N_{mem}$ (3)	$z$ (4)	$\sigma$ (km/s) (5)	Name (1)	$N_p$ (2)	$N_{mem}$ (3)	$z$ (4)	$\sigma$ (km/s) (5)
A3693	15	15	0.0921	478 +107/- 50	S463	84	84	0.0413	608 + 45/- 41
A3695	81	74	0.0903	779 + 67/- 49	S753	32	32	0.0142	536 +127/- 88
A3703a	17	17	0.0743	472 + 87/- 61	S805	119	118	0.0160	541 + 57/- 43
A3703b	13	13	0.0923	554 +122/- 55	S987	33	29	0.0717	677 +141/- 66
A3705	40	40	0.0906	877 + 73/- 74	AWM1	37	14	0.0287	442 +119/- 41
A3716N	43	43	0.0493	466 + 75/- 58	AWM4	23	23	0.0328	119 + 89/- 39
A3716S	73	69	0.0458	803 + 58/- 47	AWM7	33	33	0.0178	864 +110/- 80
A3733	41	41	0.0398	608 +109/- 60	C67	27	24	0.0587	581 +136/- 92
A3744	73	57	0.0390	508 + 74/- 48	CL2335- 26	36	29	0.1249	601 +115/- 63
A3764	38	35	0.0766	593 upp. lim.	DC0003- 50	35	24	0.0356	348 + 54/- 40
A3809	95	71	0.0631	478 + 62/- 45	Eridanus	54	54	0.0058	264 + 29/- 27
A3822	83	77	0.0769	810 + 89/- 58	MKW1	15	15	0.0198	227 + 87/- 37
A3825	63	59	0.0760	699 + 79/- 58	MKW3S	30	30	0.0450	610 + 69/- 52
A3879	45	40	0.0679	398 + 60/- 36	MKW4	51	51	0.0198	525 + 71/- 48
A3921	31	29	0.0944	490 +126/- 73	MKW5	20	20	0.0246	0 +135/- 0
A4008	27	27	0.0558	427 + 64/- 42	MKW6A	13	13	0.0257	273 + 83/- 31
A4010	28	28	0.0966	625 +127/- 95	MKW10	17	17	0.0201	161 + 42/- 20
A4053	16	16	0.0729	615 +212/- 79	MKW12	16	16	0.0198	233 +101/- 29
A4067	29	17	0.0998	499 +123/- 74	Ursa	57	57	0.0032	128 + 17/- 11
S84	19	17	0.1086	329 + 60/- 25	Virgo	436	179	0.0038	632 + 41/- 29
S373	57	57	0.0499	310 + 30/- 25					

TABLE 3  
THE RESULTS OF MORPHOLOGICAL ANALYSIS

Name (1)	$N_e$ (2)	$N_t$ (3)	$P_m$ (4)	$P_F$ (5)	References (6)
A119	58	14	0.976	0.955	Fab105,788
A151b	6	5	0.370	>0.999	Dre42,565
A194	38	25	0.644	0.989	Chi214,351
A229*	21	8	0.395	0.997	E
A400	57	24	0.994	0.596	PCG;But57,665;Dre42,565
A496	54	17	0.991	0.396	Dre42,565
A524*	5	5	0.977	0.905	E
A548NE*	61	30	0.982	0.624	E;Dre95,284
A1060 Hydra	81	54	0.993	0.395	Ric67,237;Ric77,237
A1775a	9	11	0.794	0.996	Oeg110,1
A2142*	76	9	0.107	0.973	Oeg110,1
A2151 Hercules	51	41	0.989	0.094	Dre95,284
A2634	64	22	0.427	>0.999	Dr42,565
A2819a*	25	10	0.840	0.995	E
A3381	16	8	0.581	0.957	Dre95,284
A3651*	60	7	0.911	>0.999	E
A3744*	56	6	0.326	0.994	E
A3809*	70	16	0.109	0.995	E
DC0003-50	22	11	0.864	0.974	Dre95,284
Virgo	178	244	0.128	>0.999	Bin90,1681

NOTE.— An asterisk indicates that spectral information is used. The references for spectral features are the same as for galaxy redshifts. We refer to Table 1 for the code used in the references.



TABLE 4  
THE  $\sigma$  VALUES FOR MULTYPEAKED CLUSTERS

Name (1)	$N_p$ (2)	$N_{mem}$ (3)	$z$ (4)	$\sigma$ (km/s) (5)
A13	37	37	0.0950	896 + 85/-73
A87	19	19	0.0568	511 + 98/-33
A118	26	26	0.1155	622 + 84/-57
A168	75	65	0.0451	435 + 31/-24
A957	44	44	0.0436	659 + 88/-56
A1367	84	84	0.0216	798 + 75/-68
A1651	30	30	0.0844	1006 +118/-92
A1736a	36	34	0.0347	415 + 75/-42
A1736bc	63	63	0.0461	854 + 70/-52
A2052	45	45	0.0356	520 + 55/-47
A2854	20	20	0.0622	367 + 74/-76
A3112	66	62	0.0757	552 + 86/-63
A3202	26	26	0.0698	443 + 59/-37
A3341	64	64	0.0379	585 + 55/-38
A3526	263	156	0.0114	791 + 60/-62
A3806	98	81	0.0777	771 + 55/-50
A4038	60	60	0.0302	847 + 77/-49
Pegasus	76	76	0.0140	780 + 47/-52

TABLE 5  
THE  $\sigma$  VALUES FOR MULTYPEAKED CLUSTERS (DISJOINED PEAKS)

Name (1)	$N_p$ (2)	$N_{mem}$ (3)	$z$ (4)	$\sigma$ (km/s) (5)
A13a	21	21	0.0972	515 +104/-81
A13b	16	16	0.0919	361 + 53/-35
A87a	13	13	0.0558	224 + 55/-24
A118a	13	13	0.1137	187 + 40/-28
A118b	13	13	0.1172	335 +127/-64
A168a	25	25	0.0469	118 + 27/-16
A168b	29	29	0.0436	160 + 30/-19
A168c	21	21	0.0454	88 + 16/-13
A957a	21	21	0.0416	254 + 86/-41
A957b	23	23	0.0457	481 +107/-66
A1367a	68	68	0.0221	570 + 72/-62
A1651a	20	20	0.0863	685 +129/-99
A1651c	10	10	0.0805	363 +182/-74
A1736a	36	34	0.0347	415 + 75/-42
A1736b	37	37	0.0439	569 + 54/-38
A1736c	26	26	0.0493	456 + 61/-40
A2052a	28	28	0.0346	207 + 41/-26
A2854a	14	14	0.0619	130 + 32/-26
A3112b	13	13	0.0735	86 + 33/-17
A3202a	16	16	0.0708	250 + 43/-26
A3202b	10	10	0.0683	179 +133/-37
A3341a	43	43	0.0390	351 + 52/-39
A3341b	21	21	0.0356	209 + 30/-25
A3526a	185	121	0.0108	447 + 56/-36
A3526b	78	41	0.0157	289 + 59/-31
A3806a	56	56	0.0762	502 + 66/-56
A3806b	29	27	0.0808	297 + 47/-28
A4038a	40	40	0.0285	413 + 65/-40
A4038b	20	20	0.0339	337 + 72/-41
Pegasus-a	37	37	0.0130	288 + 43/-16
Pegasus-b	27	27	0.0169	223 + 51/-44

TABLE 6  
 $\sigma$  vs. ABELL RICHNESS  $R$

$R$ (1)	$N$ (2)	$\sigma$ (km/s) (3)
-1	6	500±61
0	22	485±45
1	69	587±28
2	34	770±45
3	7	807±64